REPORT DOCUMENTATION PAGE

Form Approved OMB NO. 0704-0188

1. REPORT DATE (DD-MM-YYYY)	2. REPORT TYPE	3. DATES COVERED (From - To)
	New Reprint	-

4. TITLE AND SUBTITLE
Channel modelling and performance of non-line-of-sight ultraviolet scattering communications

5a. CONTRACT NUMBER
W911NF-09-1-0293

5b. GRANT NUMBER

5c. PROGRAM ELEMENT NUMBER
611102

6. AUTHORS
H. Ding, G. Chen, Z. Xu, B.M. Sadler

5d. PROJECT NUMBER

5e. TASK NUMBER

5f. WORK UNIT NUMBER

7. PERFORMING ORGANIZATION NAMES AND ADDRESSES
University of California - Riverside
200 University Office Building

Riverside, CA 92521 -0001

8. PERFORMING ORGANIZATION REPORT NUMBER

9. SPONSORING/MONITORING AGENCY NAME(S) AND ADDRESS (ES)
U.S. Army Research Office
P.O. Box 12211
Research Triangle Park, NC 27709-2211

10. SPONSOR/MONITOR'S ACRONYM(S)
ARO

11. SPONSOR/MONITOR'S REPORT NUMBER(S)
56047-NS.10

12. DISTRIBUTION AVAILIBILITY STATEMENT
Approved for public release; distribution is unlimited.

13. SUPPLEMENTARY NOTES
The views, opinions and/or findings contained in this report are those of the author(s) and should not contrued as an official Department of the Army position, policy or decision, unless so designated by other documentation.

14. ABSTRACT
The solar blind ultraviolet (UV) spectrum shows unique properties for wireless communication and sensing. Sufficient scattering in UV spectrum can make a non-line-of-sight (NLOS) communication scenario feasible. We present recent experimental and analytical results in non-line-of-sight UV channel modeling, including impulse response and path loss. We further study the NLOS UV link performance for short range scenarios based on our theoretical modeling method. Geometry based path loss results are presented. Tradeoffs between transmitter power and channel bandwidth are examined. Useful link budget results are proposed and analyzed for long range

15. SUBJECT TERMS
Channel modelling, Ultraviolet scattering communication, performance

16. SECURITY CLASSIFICATION OF:			17. LIMITATION OF ABSTRACT	15. NUMBER OF PAGES	19a. NAME OF RESPONSIBLE PERSON
a. REPORT	b. ABSTRACT	c. THIS PAGE			Gang Chen
UU	UU	UU	UU		19b. TELEPHONE NUMBER 951-827-2953

Report Title

Channel modelling and performance of non-line-of-sight ultraviolet scattering communications

ABSTRACT

The solar blind ultraviolet (UV) spectrum shows unique properties for wireless communication and sensing. Sufficient scattering in UV spectrum can make a non-line-of-sight (NLOS) communication scenario feasible. We present recent experimental and analytical results in non-line-of-sight UV channel modeling, including impulse response and path loss. We further study the NLOS UV link performance for short range scenarios based on our theoretical modeling method. Geometry based path loss results are presented. Tradeoffs between transmitter power and channel bandwidth are examined. Useful link budget results are proposed and analyzed for long range communication links up to 5 kilometers.

REPORT DOCUMENTATION PAGE (SF298)
(Continuation Sheet)

Continuation for Block 13

ARO Report Number 56047.10-NS
Channel modelling and performance of non-line...

Block 13: Supplementary Note

Approved for public release; distribution is unlimited.

www.ietdl.org

Published in IET Communications
Received on 13th January 2011
Revised on 21st July 2011
doi: 10.1049/iet-com.2011.0026

In Special Section: Photonic and Free Space Optics Networks

ISSN 1751-8628

Channel modelling and performance of non-line-of-sight ultraviolet scattering communications

H. Ding[1] *G. Chen*[1] *Z. Xu*[2] *B.M. Sadler*[3]

[1]*Department of Electrical Engineering, University of California, Riverside, CA 92521, USA*
[2]*Department of Electronic Engineering and Tsinghua National Laboratory & Information Science and Technology (TNLIST)*
[3]*Army Research Laboratory, Adelphi, MD 20783, USA*
E-mail: dinghaipeng@gmail.com; gachen@ee.ucr.edu; xuzy@tsinghua.edu.cn; brian.m.sadler6.civ@mail.mil

Abstract: The solar-blind ultraviolet (UV) spectrum has useful properties for wireless communication and sensing. Strong atmospheric scattering in the UV spectrum enables non-line-of-sight (NLOS) communication. The authors present recent experimental and analytical results in NLOS UV channel modelling, including impulse response and path loss. The authors further study the NLOS UV link performance for short-range communication scenarios based on our theoretical modelling results. Relations between power limitation and channel bandwidth limitation are examined. Some link budget results are analysed for long-range communication links up to 5 km.

1 Introduction

Ultraviolet (UV) signal propagation in the atmosphere has useful properties such as strong atmospheric scattering and attenuation, and solar blindness in the deep UV band (wavelength 200–280 nm). Scattering enables non-line-of-sight (NLOS) communications, whereas attenuation ensures signal extinction at longer ranges. With low to negligible solar radiation background short-range UV link performance is dominated by scattering and absorption.

UV communications has a rich history (see the survey in [1]). A series of relevant studies on UV communication have been conducted since the 1960s, mainly for longer ranges [2–5]. Those early NLOS UV studies employed flashtube and lamp sources that had significant limits in bandwidth and generally consumed high power. Recent progress in semiconductor optical sources and detectors promises low power and cost, as well as high bandwidth. Research grade light-emitting diodes (LEDs) are available, and commercial high-gain UV photomultiplier tubes (PMTs) with large detection area enable high-detection sensitivity for very weak signals. Avalanche photodiode (APD) detectors are also rapidly being developed [6, 7]. These device advances have inspired recent research in LED-based short-range NLOS UV communication systems [8, 9].

The study on NLOS UV communication channels focuses on photon interactions with the atmosphere, including scattering, absorption and turbulence. Turbulence is generally ignored at relatively short ranges in clear weather conditions, so that scattering and absorption effects are of primary interest. An analytical single scattering model was developed for channel impulse response by Reilly and Warde [10]. This single scattering model was further extended to describe angular spectra and path losses [11], and an approximation provides analytically tractable analysis [12]. However, the single scattering models cannot always predict accurate communication performance. As the communication range is increased, or under dense atmospheric conditions, multiple scattering may have a more noticeable contribution to the total received signal. Based on experimental path loss measurements, an empirical path loss model leads to improved path loss prediction when compared with the single scattering theory [13]. A Monte Carlo (MC) simulation technique was suggested to develop both path loss and impulse response models [14], explicitly incorporating the multiple scattering events. A further step was taken to develop an analytical path loss model based on the probability theory governing random migration of photons in the atmosphere, undergoing scattering and absorption [15].

In this paper, we summarise our recent progress in UV communications, including channel modelling, experimentation, and link performance study [16], and also provide new performance study for NLOS UV links. We present NLOS link geometry and atmospheric optical properties in Section 2. Then we review some recent progress, and present new experimental and analytical impulse response and path loss results for outdoor NLOS UV communication channels in Section 3. The impulse response modelling describes UV pulse broadening via multiple scattering propagation, and path loss provides a means to assessing receiver performance through the average signal-to-noise ratio (SNR). Both the impulse response and path loss are critical to communication system design and performance assessment. Although pulse broadening creates inter-symbol interference (ISI) that limits the achievable rate for a given link, the SNR becomes

dominant in many cases of interest owing to the very high scattering and absorption losses. An analytical path loss model is developed, similar to the MC photon tracing technique [14]. The modelling results are also compared with the experimental measurements, including path loss and channel impulse response, for varying pointing geometries and baseline range. In Section 4, we further study the link performance for short- and long-range NLOS UV communications, including path loss and power requirement assessment, and power and bandwidth trade-offs.

Compared with our previous work, this paper provides more comprehensive path loss performance analysis by considering various geometry parameters, including pointing angles, FOV and baseline ranges. By simulation study of NLOS UV channel bandwidth, we also show that NLOS UV links are typically power limited to achieve certain data rate and range requirements.

2 NLOS UV communication channel

The NLOS UV channel involves a variety of phenomena, including molecular scattering and absorption, aerosol scattering and absorption, and atmospheric turbulence. For NLOS UV communications scattering serves as the vehicle for information exchange between the transmitter (Tx) and receiver (Rx). The scattered light that reaches the receiver depends on the link geometry and the optical properties of the atmosphere, as described next.

2.1 Link geometry

Consider a typical NLOS communication geometry [11, 12], as shown in Fig. 1. Denote the Tx beam full-width divergence angle by α_1, the Rx field-of-view (FOV) angle by α_2, the Tx elevation angle by β_1, Rx elevation angle by β_2, the Tx and Rx baseline separation by r and the distances of the intersected (overlap) volume V to the Tx and Rx by r_1 and r_2, respectively. Experimentally, we employ a laser or LED array with a full beam angle of 3 mrad and 17°, respectively. The PMT together with a solar-blind filter in our test-bed has an FOV angle of 30°.

2.2 Atmospheric optical properties

To describe the propagation conditions, we assume a homogeneous atmosphere and adopt the following coefficients [10]: the Rayleigh (molecular) scattering coefficient k_s^{Ray}, Mie (aerosol) scattering coefficient k_s^{Mie}, absorption coefficient k_a and extinction coefficient k_e. The total scattering coefficient is defined as the sum of the two scattering coefficients $k_s = k_s^{Ray} + k_s^{Mie}$, and the extinction coefficient is given by the sum of the scattering and absorption coefficients $k_e = k_s + k_a$. In this paper we assume gas concentrations and optical features of the atmosphere as described by Table II of [4] at wavelength 260 nm, given in Table 1.

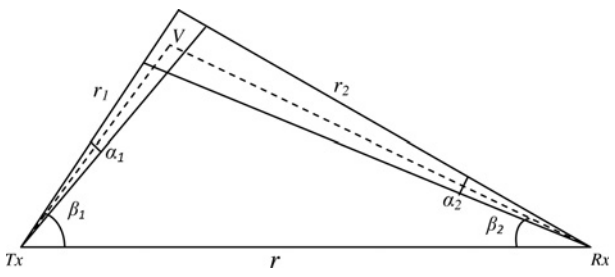

Fig. 1 *NLOS UV communication link geometry, depicting elevated transmitter beam and receiver FOV [12]*

The phase function is modelled as a weighted sum of Rayleigh (molecular) and Mie (aerosol) scattering phase functions based on the corresponding scattering coefficients [12]. This function probabilistically models the scattering properties of the atmosphere. In our simulations, we use the optical phase function given by

$$P(\mu) = \frac{k_s^{Ray}}{k_s} p^{Ray}(\mu) + \frac{k_s^{Mie}}{k_s} p^{Mie}(\mu) \tag{1}$$

where $\mu = \cos\theta_s$ is defined from the scattering angle θ_s. The two-phase functions follow a generalised Rayleigh model and a generalised Henyey–Greenstein function, respectively

$$p^{Ray}(\mu) = \frac{3[1 + 3\gamma + (1-\gamma)\mu^2]}{16\pi(1+2\gamma)} \tag{2}$$

$$p^{Mie}(\mu) = \frac{1-g^2}{4\pi}\left[\frac{1}{(1+g^2-2g\mu)^{3/2}} + f\frac{0.5(3\mu^2-1)}{(1+g^2)^{3/2}}\right] \tag{3}$$

where γ, g and f are model parameters.

3 Impulse response and path loss results

In this section, we present our analytical and experimental results for intensity impulse response and path loss.

3.1 Experimental impulse response

Fig. 2 depicts our solar-blind UV communication impulse response test bed [17]. To obtain reliable impulse response measurements, we employed a high-power UV laser capable of transmitting short pulses, and a high-sensitivity UV PMT detector combined with a solar-blind filter with a high out-of-band rejection ratio to suppress out-of-band optical noise. The system captured the measured impulse response directly in the time domain.

The transmitter employed a compact Q-switched fourth harmonic Nd:YAG laser triggered by a rectangular pulse at 10 Hz from a signal generator, producing a laser pulse train with pulse width of (3–5) ns. At the receiver, we considered both APDs and PMT detectors. The detector was followed by a customised preamplifier module. A 3 GHz digital oscilloscope was used to view and record the receiver output waveform. We first tested both detectors with LOS geometry at negligible range. Fig. 3 shows the results. We can see that the full-width half-maximum (FWHM) pulse width using the APD is less than 5 ns. The ripple in the tail was mainly caused by electric discharge in the circuit. Although the APD has a fast response time of 1 ns, its relatively small active area limits gain to only about 10^2–10^4. Consequently, the APD is not suitable for many NLOS measurement scenarios owing to an inability

Table 1 Atmosphere model parameters

λ, nm	k_s^{Ray}, km^{-1}	k_s^{Mie}, km^{-1}	k_a, km^{-1}
260	0.266	0.284	0.802

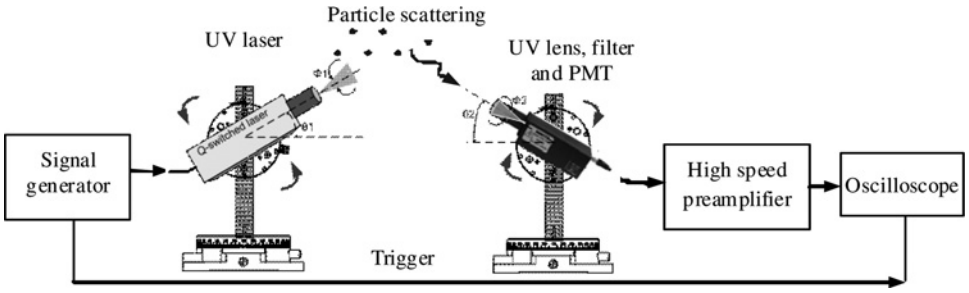

Fig. 2 *NLOS UV channel impulse response measurement system [17]*

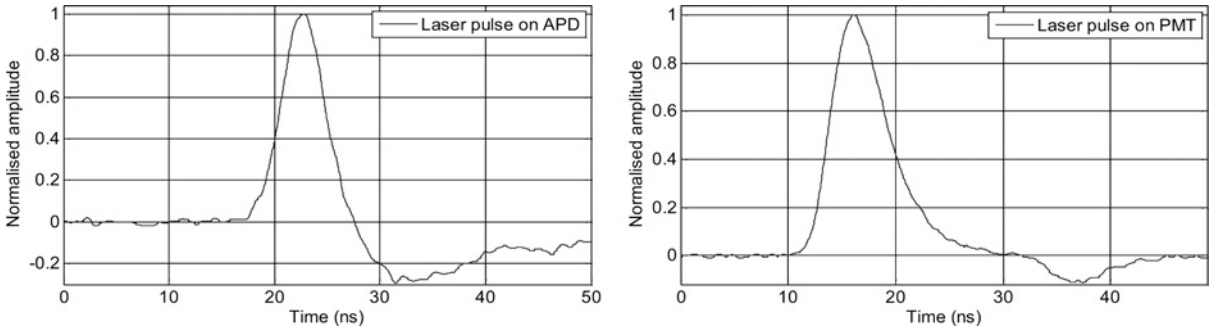

Fig. 3 *Measured pulse response [17]*

to capture weak signals. Although the PMT has a very high gain 10^5–10^7, its multiple electrode structure tends to spread the response time. The fastest commercial UV PMT available at the time of experiment was a Hamamatsu PMT whose response time was about 6 ns. The FWHM pulse width is 6.2 ns, and this represents the minimum time resolution in our channel response measurements because of non-ideal devices in the system, including the laser, detector and amplifier circuit. However, the measured channel response typically spanned from tens to hundreds, and up to thousands of nano-seconds, depending on link geometry. So, the recorded waveforms are reasonable representations of the corresponding impulse responses.

We conducted a series of tests with varying geometry, including varying Tx and Rx elevation angles from 0 to 90°, changing Tx beam angle, Rx FOV and baseline distance up to 100 m. The experimental site was an outdoor open field, with measurements conducted in daylight and clear weather. Measured waveform shapes change with varying geometry; we will present results in typical scenarios in the next subsection while leaving more extensive results to be reported elsewhere. A general observation is that a larger elevation angle induces a longer tail in the impulse response. This arises as the overlap volume increases, yielding a larger spatial spread of scattering interactions and correspondingly extending delay spread in the impulse response.

3.2 Simulated impulse response

The simulation method described here can compute the impulse response because of multiple scattering via MC simulation of each photon's arrival probabilities and the associated propagation delay to the Rx.

The main idea of the MC method is to simulate a complex process as a succession of elementary events whose probability laws are known. Light is decomposed into a set of photons and each individual photon's migration process is probabilistically modelled. The process is repeated for a large number of photons, yielding a statistical picture of the propagation channel. After emission, each photon will follow a migration path where it may be scattered and absorbed. The length of each migration is governed probabilistically, as is the next scattering angle. Each photon has an initial survival probability that is renewed after each migration. The photon is repeatedly migrated until it either reaches the receiver or its survival probability is smaller than a threshold value whereupon it is considered lost. The process is repeated for many photons, and the aggregated arrival probabilities, as a function of time, represent the expected received signal intensities, corresponding to the channel impulse response. A detailed description of this model is available in [14].

To validate our MC impulse response model, we compare our simulated impulse response with our measured response for varying pointing angles with a baseline range of 100 m as shown in Fig. 4. We observe that the pulse spreading is roughly 200, 300, 400, 500 ns for these four pointing geometries. There is a reasonable agreement between the simulation and experimental results. However, scenarios with small pointing angles have shown larger errors between the measurement and simulation, and we continue to investigate these cases. We conjecture that the mismatch between experiment and prediction may be attributed to system calibration errors, inaccurate atmospheric parameters for the system operating conditions and other measurement errors.

3.3 Experimental path loss

Motivated by analytical path loss expressions under a single scattering assumption, we postulated the following general form for the measured path loss [12]

$$\mathrm{PL} = \xi r^{\alpha} \tag{4}$$

doi: 10.1049/iet-com.2011.0026

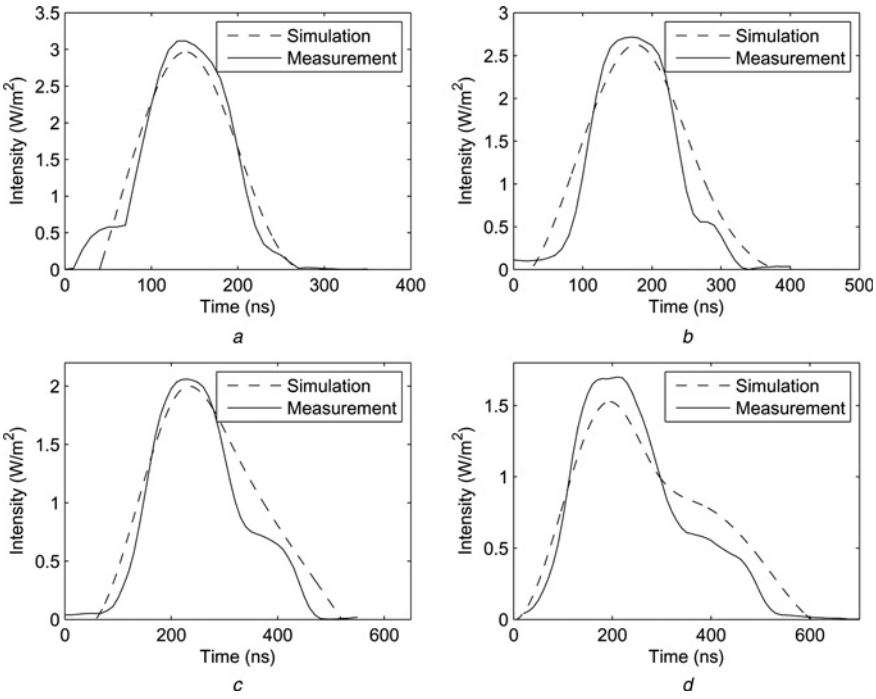

Fig. 4 *Comparison of simulated and measured impulse responses [18]*

a Impulse response for $(\beta_1, \beta_2) = (45^\circ, 40^\circ)$
b Impulse response for $(\beta_1, \beta_2) = (45^\circ, 60^\circ)$
c Impulse response for $(\beta_1, \beta_2) = (45^\circ, 80^\circ)$
d Impulse response for $(\beta_1, \beta_2) = (45^\circ, 90^\circ)$

where the path loss factor ξ and path loss exponent α are implicitly functions of the pointing angles. The term r^α stems from free space path loss. Parameter α takes a value of two for a point source in a free space LOS link, but reduces to approximately one in large pointing angle geometries ($\beta_1 = \beta_2 > 60^\circ$) [13]. Note, however, that ξ also changes with angle geometry, over several orders of magnitude. Both parameters were estimated by a curve-fitting technique based on our extensive field-test path loss results, as a function of pointing angles and baseline range. The results were tabulated and described in [13].

We have validated the path loss predictions by comparing with independent measurements, using a relatively low-powered LED source array. A high-powered source is needed at longer ranges, especially with large pointing angles (approaching vertical) where the path loss becomes very large. Consequently, our measurements at ranges up to 100 m required small (low to the horizon) pointing angles, whereas at shorter baseline distances we were able to measure path loss at larger angles. Fig. 5 compares predicted and measured path losses for Tx and Rx apex angles up to 40° with a baseline separation of 100 m. The prediction errors for each Tx elevation angle are within a few decibels over the specified range of the Rx elevation angle, which illustrates that our empirical model provides a good prediction for ranges up to 100 m with small to medium pointing angles. Fig. 6 compares path loss measurement and simulation assuming single scattering. The model parameters matched the experimental measurement system as closely as possible, and assumed a tenuous atmosphere, with the measurements taken outdoors on a clear day. The simulation shows a reasonable agreement, within a few dB. In general, as expected, we observe that the loss increases as either the Tx or Rx angle increases. This is due to the longer propagation path as well as the inherent scattering loss.

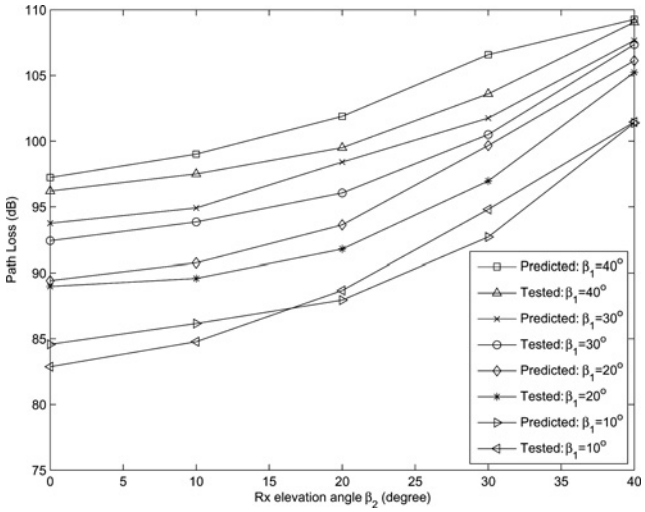

Fig. 5 *Comparison of predicted and tested path losses for different Tx and Rx angles at 100 m distance [13]*

3.4 Analytical path loss model

Following the same physical scattering law as the MC simulation [14], here we propose a stochastic analytical method to theoretically derive the *n*th order scattered signal energy collected by the detector [15]. The model considers all photons stochastically scattered and absorbed by the atmospheric particles, and involves probabilistic modelling of photon random moving direction, distance, energy loss and receiver capture after a certain number of scatterings. In order to obtain the *n*th-order scattered signal at the receiver, we trace the migration routes of a single photon through the medium [19].

This model offers an analytical formulation for NLOS scattering channel path loss, whereas following the same

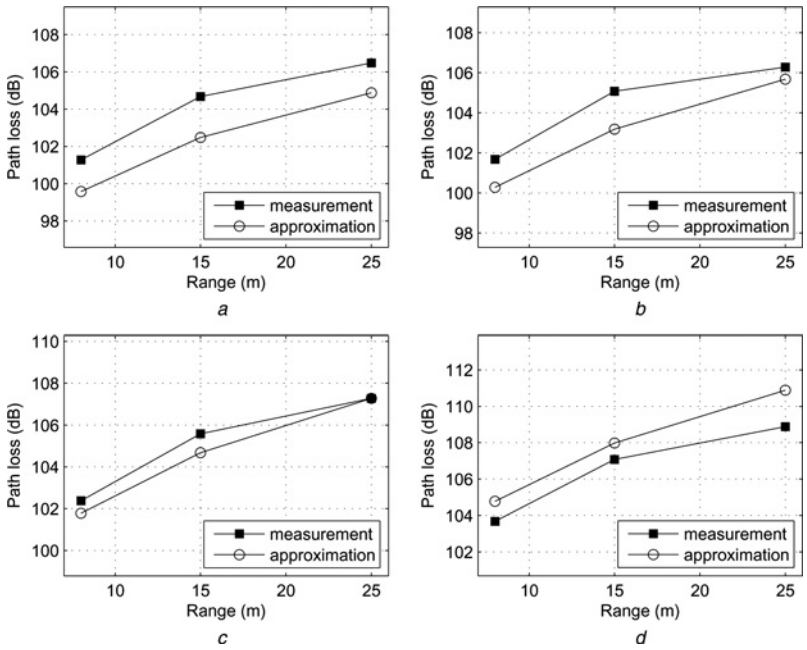

Fig. 6 *Comparison of measured and simulated path loss with four different pointing angle pairs*

a Path loss for $(\theta_1, \theta_2) = (80^\circ, 60^\circ)$
b Path loss for $(\theta_1, \theta_2) = (80^\circ, 70^\circ)$
c Path loss for $(\theta_1, \theta_2) = (80^\circ, 80^\circ)$
d Path loss for $(\theta_1, \theta_2) = (80^\circ, 90^\circ)$

probability theory as the MC method. We will show that both models match well. A detailed description of this model is available in [15]. The model assumes that the photons are stochastically scattered and/or absorbed by the atmospheric particles and involves probabilistic modelling of photon random moving direction, distance, energy loss and receiver capture after a specified number of scatterings.

Fig. 7 compares the path loss results generated from our stochastic model and the MC simulation model. Four sets of Tx and Rx elevation angles are included for detailed comparison. For each subplot, the stochastic model provides a good match with the simulation model, with modest error within 1 dB. This indicates that our proposed model is a good reference for evaluating the MC simulation model.

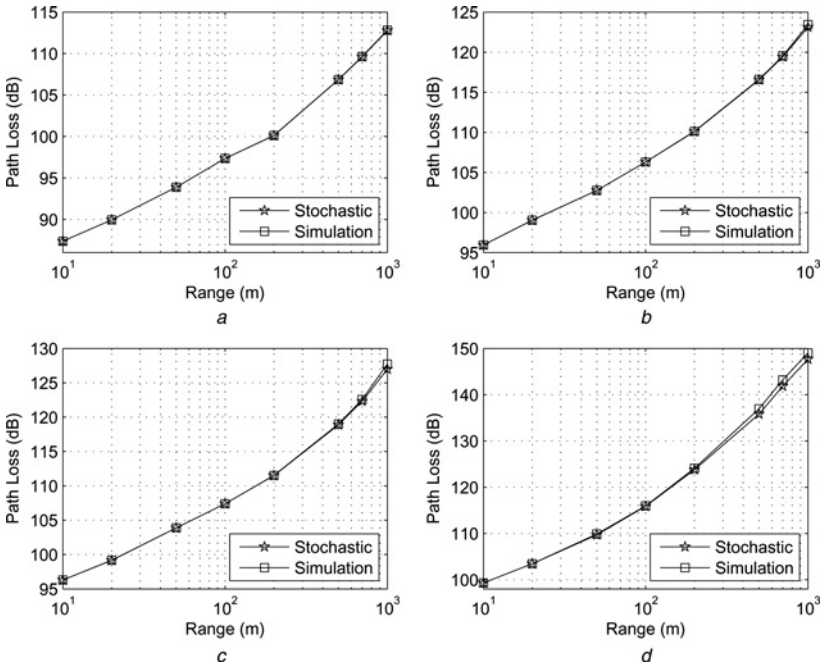

Fig. 7 *Predicted path loss of stochastic model and simulation [15]*

a Path loss for $(\beta_1, \beta_2) = (20^\circ, 20^\circ)$
b Path loss for $(\beta_1, \beta_2) = (45^\circ, 45^\circ)$
c Path loss for $(\beta_1, \beta_2) = (60^\circ, 60^\circ)$
d Path loss for $(\beta_1, \beta_2) = (90^\circ, 90^\circ)$

doi: 10.1049/iet-com.2011.0026

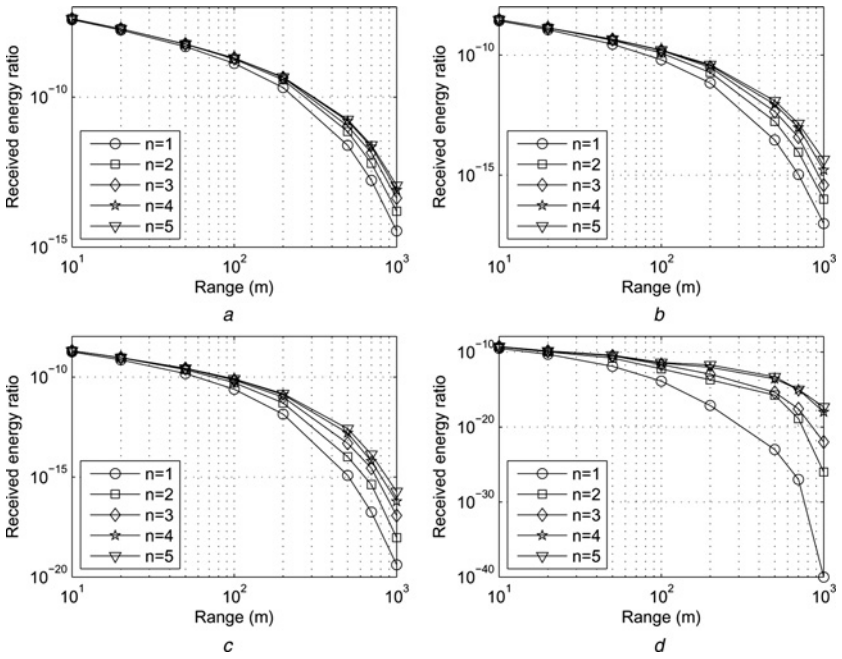

Fig. 8 *Received energy ratio for extra thick atmosphere predicted by the proposed model [15]*

a Received for $(\beta_1, \beta_2) = (20^\circ, 20^\circ)$
b Received for $(\beta_1, \beta_2) = (45^\circ, 45^\circ)$
c Received for $(\beta_1, \beta_2) = (60^\circ, 60^\circ)$
d Received for $(\beta_1, \beta_2) = (90^\circ, 90^\circ)$

In order to demonstrate the significance of higher order scattering, in Fig. 8 we plot the ratio of the accumulated received energy from $n = 1$ (first scattering order only) to $n = 5$ (sum of first through fifth order scatterings) for an extra thick atmosphere at different elevation angle pairs [15]. For each scenario, we find that the second-, third- and fourth-order scatterings contribute significantly to the total received energy. In particular, the second- and third-order scatterings overwhelm other-order scatterings. Furthermore, we can see that the fifth-order scattering does not contribute as much as the lower-order scatterings. When considering multiple scattering contributions, the path loss decreases as higher-order scattering contributions are added. These results indicate the remarkable property that for relatively shorter ranges, NLOS UV communications links are potentially enhanced in hazy or foggy weather owing to the increased number of scattering particles in the atmosphere.

4 Link performance study

In this section, we investigate the NLOS UV link performance by analysing link path loss, channel bandwidth, data rate and power requirement. All results here are obtained by our stochastic analytical method proposed in the previous section.

4.1 Simulated short-range path loss

Given experimental LED power limitations, we focus on ranges from 10 to 100 m. Note that path loss is not particularly sensitive to Tx beamwidth angle. We examine the path loss while varying Tx and Rx pointing angles and Rx FOV angle. In our simulations, we assume a default 17° Tx beam angle, 30° Rx FOV angle and 90° Rx pointing angle unless we explicitly specify these parameters.

Fig. 9 depicts range-dependent path loss for varying Tx and Rx pointing angles. We can see that path loss is very sensitive to the pointing angles. In particular, for fixed large Tx pointing angles increasing Rx pointing angle may exhibit dramatic path loss deterioration, which implies that it is necessary to increase the transmitted power to compensate the high channel attenuation loss problem for large pointing angle geometry. For example, for fixed transmit power, the NLOS communications range can be extended by lowering the pointing angles towards each other.

Under a solar blind assumption, a wide Rx FOV can increase the received signal power level without a significant increase in noise. We show the FOV effect for path loss in Fig. 10. Obviously, a wider Rx FOV produces lower path loss as the Rx is able to collect more scattering signal photons. For Tx and Rx pointing angle pair (60°, 90°), path loss for 100 m range shows more than 10 dB improvement by increasing the FOV from 30 to 180°. Other geometries also show significant reduction in path loss. However, in some practical scenarios where there is a non-trivial background noise, the FOV needs to be optimised to maximise the receiver SNR and consequently minimise the bit error rate (BER), as described in [20].

4.2 Power-limited or bandwidth-limited channel?

We have shown in Figs. 9 and 10 that path loss can be improved by increasing the Rx FOV as well as using small pointing angles for longer range UV links. However, increasing Rx FOV may also generate a loss of bandwidth as a result of pulse spreading. This occurs as the pointing angles and Rx FOV increase. Although a wide FOV is valuable to combat path loss, it also constrains the bandwidth as a result of the extended impulse response duration, which leads to a fundamental system trade-off between path loss and impulse response spreading. The achievable data rate depends not only on the channel bandwidth and path loss, but also on many other parameters such as transmitted optical power, background noise,

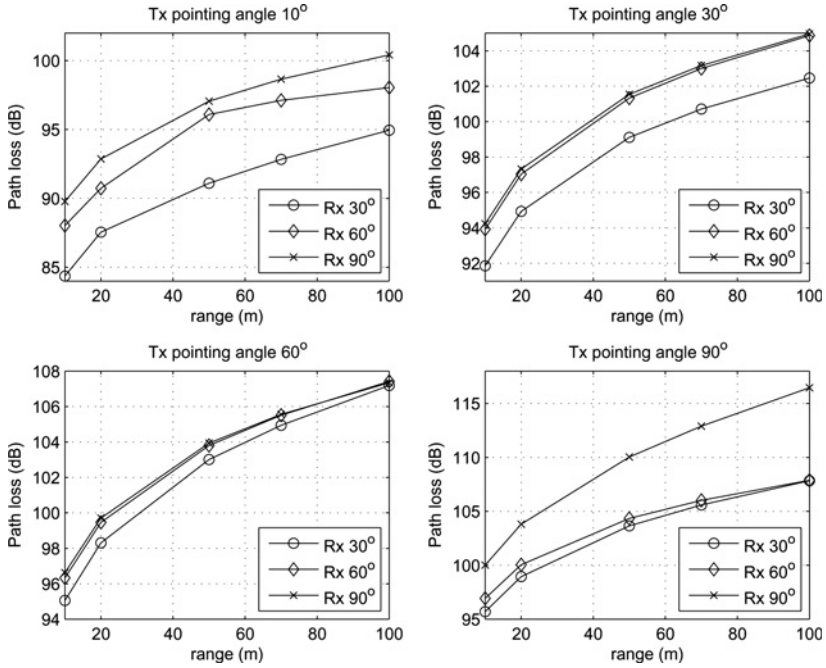

Fig. 9 *Predicted short-range path loss for varying pointing angles*

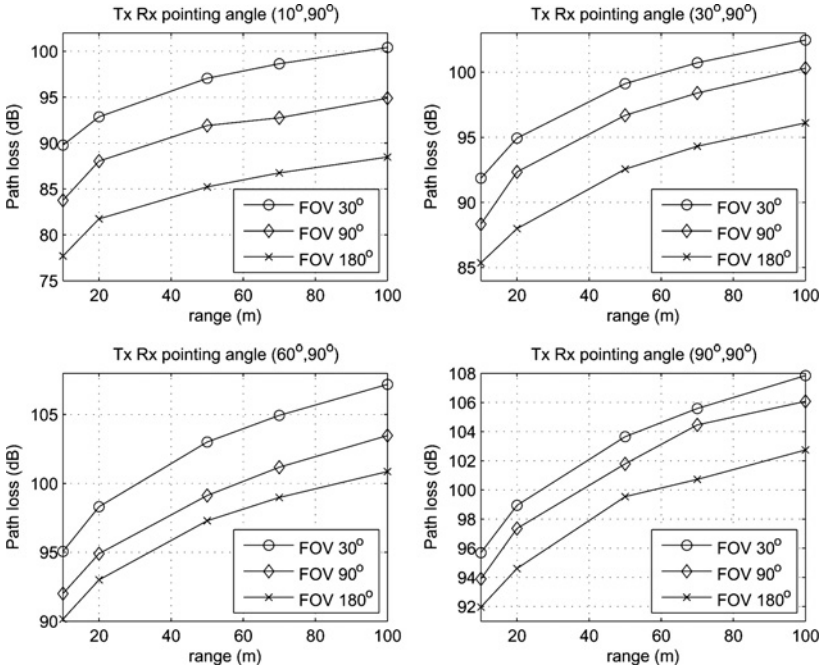

Fig. 10 *Predicted short-range path loss for varying FOV angles*

wavelength and desired BER. Here we study the achievable data rate in two respects. First, we examine the channel 3 dB bandwidth from the simulated impulse response. Then we investigate the data rate which is determined by the transmitted power, desired BER and link path loss. This reveals whether power or bandwidth is dominant in determining the achievable data rate.

We calculate the 3 dB bandwidth from the simulated channel impulse response. Fig. 11 depicts range-dependent 3 dB bandwidth for varying Tx and Rx pointing angles. We observe that bandwidth is very sensitive to the pointing angles. In particular, for fixed large Tx pointing angles, increasing Rx pointing angle may result in dramatic bandwidth deterioration, which implies limited achievable data rate for large pointing angle geometry.

Figs. 11 and 12 show the bandwidth determined by impulse response for NLOS UV links. We express the data rate by employing the formulation as described in [13]

$$R = \frac{\eta_f \eta_r P_t \lambda}{hcLN_d} \tag{5}$$

where R is the data rate, η_f is the filter transmission efficiency, η_r is the Rx detection efficiency, P_t is the transmitted power, λ is the UV wavelength, h is Planck's constant, c is the speed of light, L is the link path loss and N_d is the number of photons

doi: 10.1049/iet-com.2011.0026

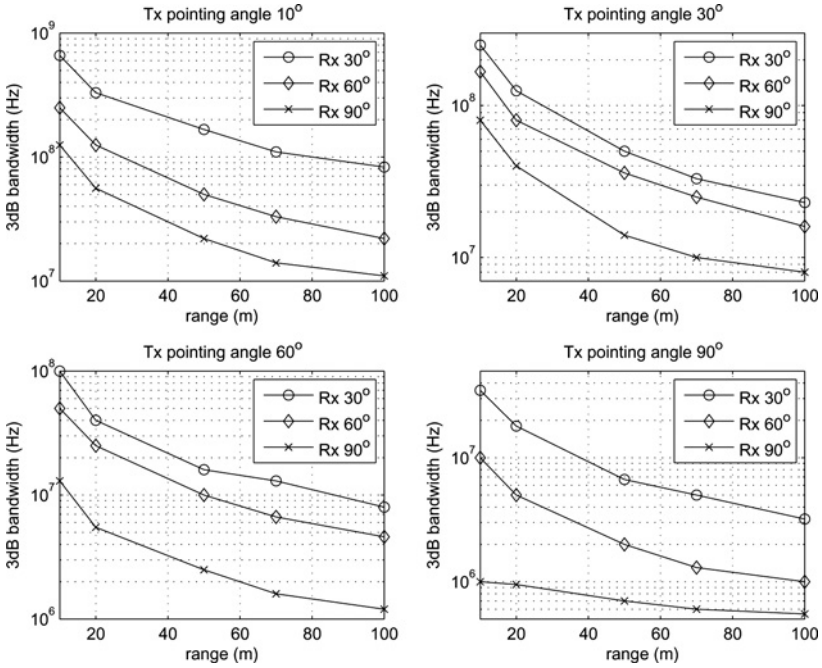

Fig. 11 *Predicted 3 dB bandwidth for varying pointing angles*

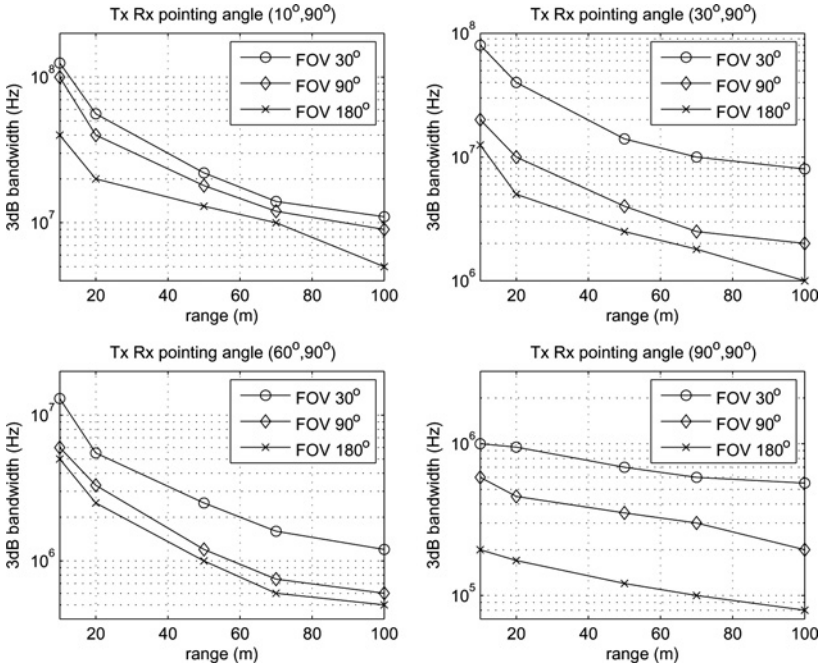

Fig. 12 *Predicted 3 dB bandwidth for varying FOV angles*

detected per pulse, N_n is the number of noise photons per pulse. Our analysis assumes an on–off keying (OOK) modulation and a medium background noise level as in [13]. Given the BER [13], N_d can be calculated from (6) and (7). Using typical experimental values, we assume the following [21]: $\eta_f = 0.2$, $\eta_r = 0.3$, $P_t = 100$ mW, $\lambda = 260$ nm and BER $= 10^{-3}$. Based on (5), we show the predicted achievable data rate for short ranges by varying pointing angles and Rx FOV as shown in Figs. 13 and 14

$$\mathrm{BER} = \frac{1}{2}\sum_{k=0}^{m_T}\frac{(N_d+N_n)^k e^{-(N_d+N_n)}}{k!} + \frac{1}{2}\sum_{k=m_T+1}^{+\infty}\frac{N_n^k e^{-N_n}}{k!} \quad (6)$$

where m_T is the optimum threshold given by an integer floor operation of a continuous variable a

$$m_T = \lfloor a \rfloor, \quad a = \frac{N_d}{\ln\{1+(N_d/N_n)\}} \quad (7)$$

Comparing Figs. 11 and 13, it is evident that the achievable data rate is dominated by path loss, where the corresponding 3 dB bandwidth for each geometry is much larger than the data rate result from (5). We have noted that while a wider Rx FOV can decrease path loss and potentially increase data rate, there is a corresponding increase in the pulse spreading. However, from Figs. 12 and 14, we can clearly see that the bandwidth

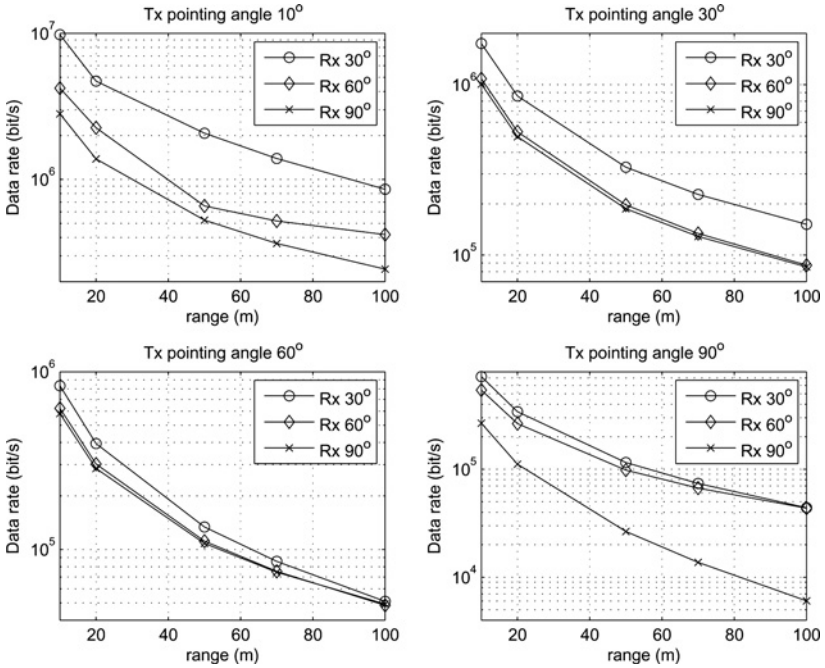

Fig. 13 *Predicted data rate for varying pointing angles*

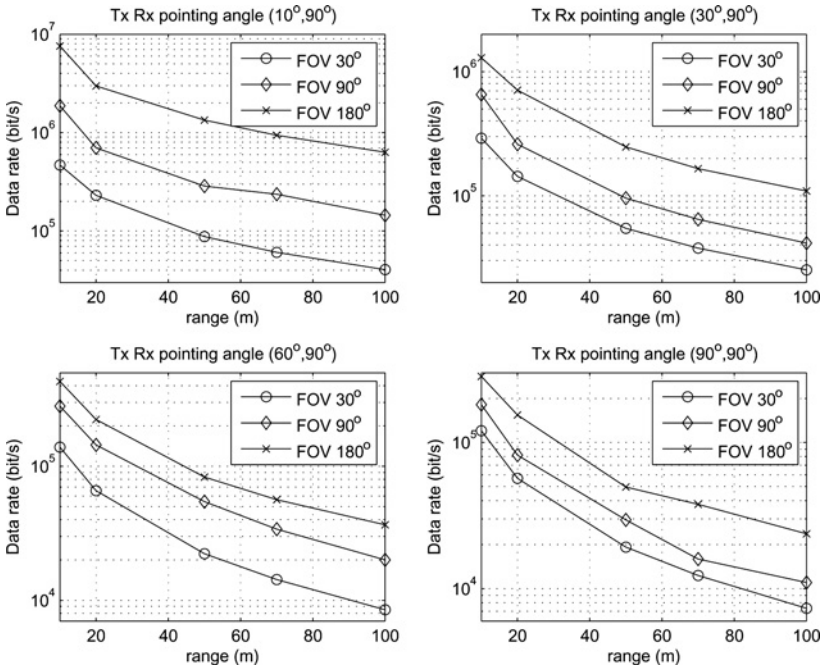

Fig. 14 *Predicted data rate for varying FOV angles*

plays a minor role in determining the data rate, because the NLOS UV link-based on current system parameters is power limited. For a given set of system parameters, the achievable data rate can be calculated using (5).

4.3 Simulated long-range path loss and power requirement

The above discussions are for short-range NLOS UV communications up to roughly 100 m. In practical scenarios, longer-range communication links (up to several kilometres) may also be desired. Although an NLOS UV communication system employing current LED source technology may have a limited communication distance, a higher-power UV laser enables a longer communication distance, although eye and skin safety becomes an issue when exposed to the direct laser beam.

In this subsection, we investigate the power requirement for long-range NLOS UV links by varying the system geometry, considering baseline range from 1 to 5 km, while varying pointing angles and FOV. Both path loss and power requirements are studied. We assume a default 3 mrad Tx beam angle, 30° Rx FOV angle and 90° Rx pointing angle unless we otherwise explicitly specify these parameters. Figs. 15 and 16 depict the predicted path loss for varying pointing angles and FOV, respectively. As for short range,

doi: 10.1049/iet-com.2011.0026

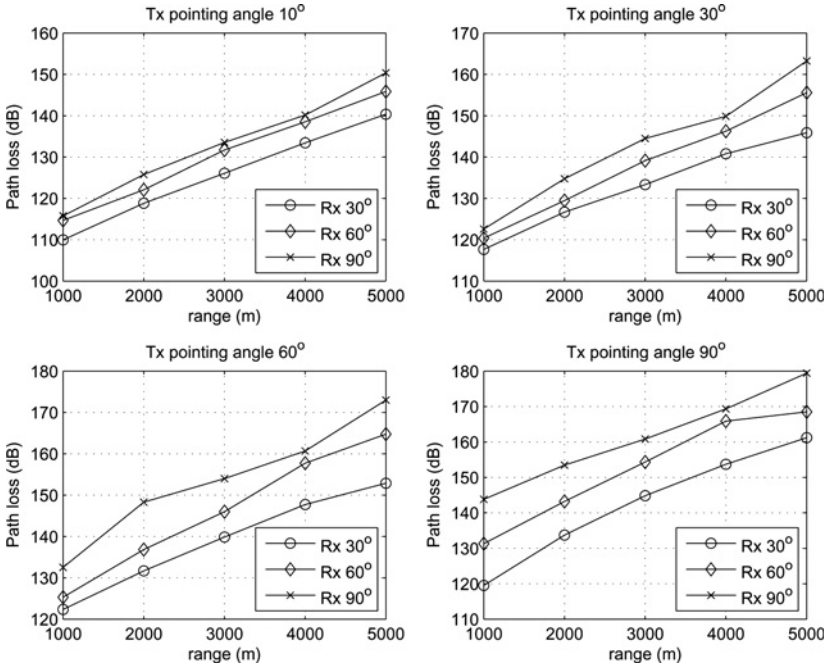

Fig. 15 *Predicted long-range path loss for varying pointing angles*

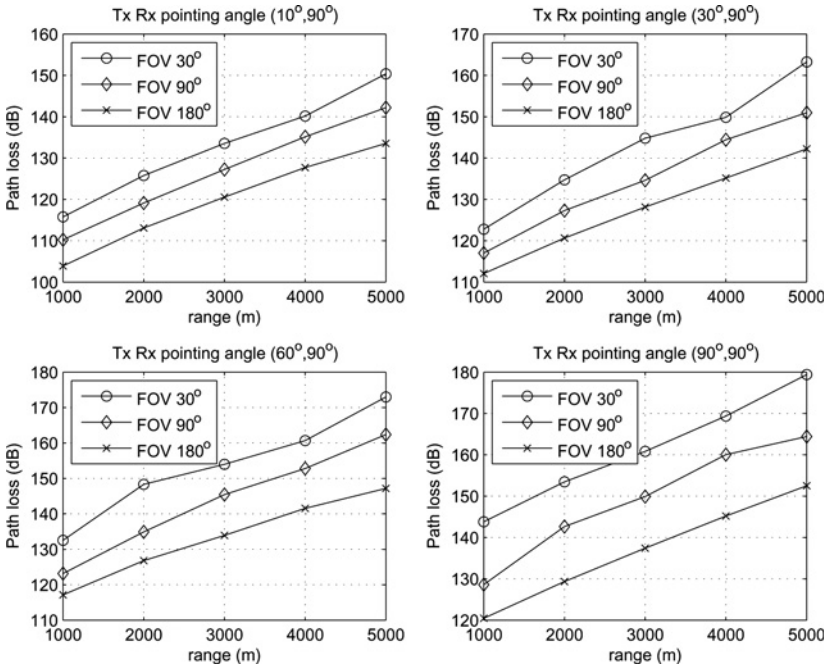

Fig. 16 *Predicted long-range path loss for varying FOV angles*

we observe that path loss is very sensitive to the pointing angles and FOV. Path loss deteriorates rapidly with increasing pointing angles at long ranges. For example, a path loss of about 180 dB is predicted for pointing angle set (90°, 90°) at a range of 5 km, a very large loss that would require a significantly powerful transmitter to overcome. In Fig. 16, large FOVs result in significant improvements for the link path loss in different geometries. For Tx and Rx pointing angle pair (60°, 90°), path loss for a 5 km range shows a 30 dB improvement by changing the FOV from 30 to 180°, although this assumes the background noise count is not increasing with enhanced FOV and ultimately it may be desirable to find a good trade-off in Rx FOV as we noted earlier.

Figs. 15 and 16 demonstrate very large path loss results for long-range links, demonstrating that at longer ranges the NLOS UV link is very much power limited. Here we further study the power requirement for long-range UV links. For given system parameters, we can derive the required transmission power from (5) to be $P_t = \{(RhcLN_d)/(\eta_f \eta_r \lambda)\}$. For fixed system parameters, we observe a linear relationship between transmitted power and path loss. For example, assuming the following parameters, $\eta_f = 0.2$, $\eta_r = 0.3$, $R = 5$ kbps, $\lambda = 260$ nm and BER $= 10^{-3}$, we obtain $P_t = 1.8704 \times 10^{-13} L$. Here we define path loss $L = P_t/P_r$, where P_t and P_r are transmitted power and received power, respectively. Based on the linear relationship, we can predict similar results for power requirement with

varying geometry. This quickly yields practical limitations on NLOS UV links. For example, for a (90°, 90°) pointing angle link at a range of 5 km, we may need more than 10^5 W power to achieve BER $= 10^{-3}$ and $R = 5$ kbps.

5 Conclusion

Incorporating experimental field-test results and analytical calculation, we presented our NLOS UV modelling methods from different viewpoints. Our models provide reasonably accurate path loss prediction for the cases studied, at baseline ranges up to 100 m, as validated by extensive outdoor measurements. For short-range UV links, we examined the path loss variations for varying geometries. We showed that an NLOS UV link is generally power-limited by a comparative study of simulated bandwidth and calculated data rate. For longer range communication links, we examined both path loss and power requirements for different geometries for ranges up to 5 km. Our results indicate that very high-path loss requires high power for large pointing angles at long ranges, although a large FOV will significantly help to improve the link conditions. These results are useful for system design and communications link performance analysis. Further topics of interest include developing an analytical impulse response model, as well as analysis of channel turbulence effects for NLOS links.

6 Acknowledgments

This work was supported in part by National Natural Science Foundation of China under Grant 61171066, Tsinghua National Laboratory for Information Science and Technology (TNLIST) Cross Discipline Foundation under Grant 2011Z02289.

7 References

1 Xu, Z., Sadler, B.M.: 'Ultraviolet communications: potential and state-of-the-art', *IEEE Commun. Mag.*, 2008, **46**, (5), pp. 67–73
2 Harvey, G.L.: 'A survey of ultraviolet communication systems'. Naval Research Laboratory Technical report, Washington, DC, March 1964
3 Sunstein, D.E.: 'A scatter communication link at ultraviolet frequencies'. BS thesis, MIT, Cambridge, MA, 1968
4 Junge, D.M.: 'Non-line-of-sight electro-optic laser communications in the middle ultraviolet'. MS thesis, Naval Postgraduate School, Monterey, CA, December 1977
5 Ross, W.S., Kennedy, R.S.: 'An investigation of atmospheric optically scattered non-line-of-sight communication links'. Army Research Office Project report, Research Triangle Park, NC, January 1980
6 Bai, X., Mcintosh, D., Liu, H., Campbell, J.C.: 'Ultraviolet single photon detection with Geiger-mode 4H-SiC avalanche photodiodes', *IEEE Photonics Technol. Lett.*, 2007, **19**, (22), pp. 1822–1824
7 Shen, S.C., Zhang, Y., Yoo, D., *et al.*: 'Performance of deep ultraviolet GaN avalanche photodiodes grown by MOCVD', *IEEE Photonics Technol. Lett.*, 2007, **19**, (21), pp. 1744–1746
8 Shaw, G.A., Siegel, A.M., Model, J., Greisokh, D.: 'Recent progress in short-range ultraviolet communication'. Proc. SPIE, Orlando, FL, March 2005, vol. 5796, pp. 214–225
9 Chen, G., Abou-Galala, F., Xu, Z., Sadler, B.M.: 'Experimental evaluation of LED-based solar blind NLOS communication links', *Opt. Express*, 2008, **16**, (19), pp. 15059–15068
10 Reilly, D.M., Warde, C.: 'Temporal characteristics of single-scatter radiation', *J. Opt. Soc. Am.*, 1979, **69**, (3), pp. 464–470
11 Luettgen, M.R., Shapiro, J.H., Reilly, D.M.: 'Non-line-of-sight single-scatter propagation model', *J. Opt. Soc. Am.*, 1991, **8**, (12), pp. 1964–1972
12 Xu, Z., Ding, H., Sadler, B.M., Chen, G.: 'Analytical performance study of solar blind non-line-of-sight ultraviolet short-range communication links', *Opt. Lett.*, 2008, **33**, (16), pp. 1860–1862
13 Chen, G., Xu, Z., Ding, H., Sadler, B.M.: 'Path loss modeling and performance trade-off study for short-range non-line-of-sight ultraviolet communications', *Opt. Express*, 2009, **17**, (5), pp. 3929–3940
14 Ding, H., Chen, G., Majumdar, A.K., Sadler, B.M., Xu, Z.: 'Modeling of non-line-of-sight ultraviolet scattering channels for communication', *IEEE J. Sel. Topics Commun.*, 2009, **27**, (9), pp. 1535–1544
15 Ding, H., Xu, Z., Sadler, B.M.: 'A path loss model for non-line-of-sight ultraviolet multiple scattering channels', *EURASIP J. Wirel. Commun. Netw.*, 2010, **2010**, pp. 1–12, article id 598572
16 Ding, H., Chen, G., Sadler, B.M., Xu, Z.: 'Characterization and modeling of non-line-of-sight ultraviolet scattering communication channels'. Proc. Seventh IEEE, IET Int. Symp. on Commun. Syst., Networks and Digital Signal Processing, UK, July 2010
17 Chen, G., Xu, Z., Sadler, B.M.: 'Experimental demonstration of ultraviolet pulse broadening in short-range non-line-of-sight communication channels', *Opt. Express*, 2010, **18**, (10), pp. 10500–10509
18 Ding, H., Chen, G., Majumdar, A.K., Sadler, B.M., Xu, Z.: 'Non-line-of-sight ultraviolet communication channel characterization: modeling and validation'. Proc. SPIE, San Diego, CA, 2009, vol. 7464, pp. 74640I-1–74640I-2
19 Gillespie, D.T.: 'Stochastic-analytic approach to the calculation of multiply scattered lidar returns', *J. Opt. Soc. Am.*, 1985, **2**, (8), pp. 1307–1324
20 Majumdar, A.K.: 'Laboratory-simulation experiment for optical communication through low-visibility atmosphere using a diode laser', *IEEE J. Quantum Electron.*, 1984, **QE-20**, (8), pp. 919–932
21 He, Q., Xu, Z., Sadler, B.M.: 'Performance of short-range non-line-of-sight LED-based ultraviolet communication receivers', *Opt. Express*, 2010, **18**, (12), pp. 12226–12238

doi: 10.1049/iet-com.2011.0026